Iron oxidation dynamics vs. temperature of synthetic potassic-ferro-richterite: a XANES investigation

G. Della Ventura,[a,b] F. Galdenzi,[a] G. Cibin,[c] R. Oberti[d], Wei Xu[e,f], S. Macis[b,g] and A. Marcelli[b,f]

We investigated the oxidation behaviour of a synthetic potassic-ferro-richterite up to 750° C by using simultaneous X-ray absorption spectroscopy and X-ray diffraction experiments with synchrotron radiation. From X-ray diffraction we observed an abrupt drop of cell dimensions ~335° C accompanied by an anomalous increase in the monoclinic cell angle β. From the analysis of the XANES spectra at the iron K-edge we observed that the structural shrinkage is due to the iron oxidation process, coupled to hydrogen loss, occurring at ~315° C, slightly before the cell contraction. Combining these results with previous studies performed on similar samples by single-crystal structure refinement, Mössbauer, High Temperature-Fourier Transform IR and Raman spectroscopies we show that the temperature evolution in Fe-amphiboles is a multi-step process. Following the iron oxidation driven by the temperature, the structural dynamics in this double-chain silicate is ruled by local strains in the ribbon of iron-filled octahedra, mainly due to the contraction of the *M*(1) site.

Introduction

Iron is the most abundant metallic element on the Earth, and has a variable oxidation state that is extremely sensitive to the geochemical environment. Characterization of its valence state is therefore important in geology to define the condition of formation of the rocks where Fe-bearing minerals are found. The Fe^{3+}/Fe^{2+} ratio of minerals is used in petrology, for example, to estimate the P, T and f_{O_2} parameters, and to provide insight into the nature of fluids in the geological system during crystallization.[1] This ratio is also widely used in mineralogy, and its evaluation is addressed typically by Mössbauer spectroscopy, a bulk analytical method that can hardly provide information at the micro-scale.[2-5]. In the last decades, wavelength-dispersive spectroscopy (WDS) has been used, although with a limited success, to estimate the Fe^{3+}/Fe_{tot} ratio in minerals, and in particular in amphiboles.[6-7] In contrast, X-ray absorption spectroscopy (XAS) has been successfully applied to study the Fe^{3+}/Fe^{2+} ratio in a variety of geological materials also at micro-scale.[8,9]

A further major issue for the analysis of the iron valence state is monitoring the behaviour of Fe-rich materials during high temperature (HT) experiments. Some important mineral reactions, like dehydration, involve the loss and subsequent migration or diffusion of hydrogen or hydrogen/oxygen species. In Fe-rich minerals and during post-crystallization processes, this loss is associated with the concurrent oxidation of iron. Among rock-forming silicates, this mechanism is well known to occur in Fe-rich amphiboles. The process has been studied in details during the 60's[10-13] because of the emerging technological relevance of materials containing these minerals for a variety of applications ranging from fire-proof textiles, to thermo-acoustic insulators, construction materials, water pipes, spare parts of electrical components, etc. According to these studies, the dehydration process is expressed as:

$$Fe^{2+} + OH^{-} = Fe^{3+} + O^{2-} + 1/2H_2 \qquad (1)$$

In the above reaction, one ferrous iron at one of the OH-coordinated *M*(1) and *M*(3) polyhedra (see Figure 1) oxidizes to ferric iron, the local charge balance being maintained by the loss of one H^{+} ion at the O(3) site.

There is also a clear evidence that this process significantly increases the electrical conductivity of the amphibole, a feature that may have significant implications, for example in geophysics, providing an explanation to the observed high conductivity in some areas of the continental crust[15] and, possibly, in material science because of the excellent stability of amphiboles up to high temperature (~900° C). Notably, this conductivity enhancement at high temperature has never been explained at the microscopic scale. As a consequence, increasing efforts have been devoted to investigate the behaviour of different amphibole compositions at non-ambient conditions[16-22]. Moreover, mechanisms and kinetics of proton diffusion throughout the mineral matrix and the role of multiple-valence elements, notably Fe, in this process are still

[a] *Department Sciences, University of Roma Tre, Rome, Italy*
[b] *INFN-LNF, P.O.Box 13, 00044 Frascati (Rome), Italy*
[c] *CNR-Istituto di Geoscienze e Georisorse, Pavia, Italy*
[d] *Diamond Light Source, Harwell Science and Innovation Campus, Didcot, UK*
[e] *BSRF, Institute of High Energy Physics, Beijing, 100049, P.R. China*
[f] *Università di Tor Vergata, Via della Ricerca Scientifica 1, 00133 Roma, Italy*
[g] *RICMASS, Rome International Center for Materials Science Superstripes, Rome, Italy.*

Electronic Supplementary Information (ESI) available: procedure of extraction of the pre-edge spectra and DOS calculations.
See DOI: 10.1039/x0xx00000x

not fully identified.[21,22]. Based on the available data, a consensus exists on the validity of equation (1) as the mechanism whereby Fe-rich amphiboles dehydrate at high temperature through a proton loss concurrent to the oxidation of ferrous iron. In this process, the reactants Fe^{2+} and OH^- are provided by the amphibole, while the necessary amount of O_2 is taken from the atmosphere. In agreement with this inference, the work of Della Ventura et al.[21] recently showed that reaction (1) is indeed inhibited either in inert atmosphere or when the crystal is embedded in KBr. Note that the amphibole structure (see Figure 1) is fully retained after the complete de-protonation.[17] For the reaction to proceed, there is the need of a continuous availability of Fe^{2+} and H at the crystal surface that must be provided by the bulk of the crystal, via some electron and proton diffusion mechanisms. This model is also in agreement with studies done on calcic amphiboles with different Fe contents by combining measurements of the electrical resistivity and Mössbauer spectroscopy.[23]

This study focuses on the behaviour of a synthetic potassic-ferro-richterite during heating. It follows the papers published on the modifications of the structure at HT[17] and the HT FTIR study of the hydrogen loss from the structure[22]. In this paper, we will discuss the evolution of the Fe^{3+}/Fe_{tot} ratio on the same sample studied in the two previous works, and clarify the dynamics of this complex system, which involve electronic, structural and molecular processes. To this purpose, we performed in situ X-ray absorption spectroscopy (XAS) simultaneously with X-ray diffraction (XRD). This approach follows similar experiments where complex structural and electronic dynamics were deciphered by the combined use of different spectroscopic techniques.[8,24-28]

Results and discussion

Materials and methods

The sample studied here was synthesized by Redhammer and Roth[29] and was kindly provided to us by G. Redhammer (Salzburg). These authors prepared three experimental batches by using slightly different experimental conditions. One crystal from the batch prepared at 700° C using NNO (nickel-nickel oxide) buffer was later characterized by Oberti et al.[17] (sample R1). The crystal-chemical formula, obtained by combining single-crystal X-ray structure refinement and Fourier Transform IR (FTIR) spectroscopy[17] is: $^{A}(K_{0.90}Na_{0.07})$ $^{B}(Ca_{0.54}Na_{1.46})$ $^{C}(Fe^{2+}_{4.22}Fe^{3+}_{0.78})$ $^{T}Si_8O_{22}$ $^{W}(OH_{1.70}O^{2-}_{0.30})$.
According to the present nomenclature scheme for amphiboles[30], the sample investigated is classified as potassic-ferro-richterite. For the present study, we had to use a sample from a second experimental batch (sample Ri15, prepared at 600° C, with the MW magnetite - wüstite O_2 buffer) having a similar composition as the one studied by Oberti et al.[17] but with a slightly different bulk Fe^{3+}/Fe^{2+} ratio.[29]

Fe K-edge XANES spectra and X-ray diffraction patterns were collected simultaneously at beamline B18, the Core-XAS bending magnet beamline at Diamond Light Source, Oxfordshire (UK). All XAS measurements were taken in transmission mode using the continuous scanning (at a maximum speed of ~1°/s) and the incident beam energy was controlled by a double Si(111) crystals monochromator. The sample was a pellet made by a mixture of ~10 mg of amphibole powders and 150 mg of boron nitride. During acquisition, the temperature was increased from room temperature (RT) up to 750° C with a rate of 5° C/minute and then decreased to RT. The entire experiment was performed within ~150 minutes. Energy was calibrated by defining the first derivative peak of a metallic Fe reference foil to be at 7,112.0 eV. XRD measurements were done simultaneously to XAS experiments to make the two sets of data fully comparable in terms of both composition and T; the same T range was explored at the energy of 8048 eV. The diffractometer available at B18 is composed by six Mythen-II Si micro-strip detection modules,[31] each covering an angular range of 10°. They are arranged to cover an angle of 60° within 40 cm radius. Because the diffractometer is composed of six different modules, their assembly leaves small blind angles (~0,5° for each feature) that may reduce the amount of reflections collected without, however, significantly affecting the refinement of the unit-cell parameters.

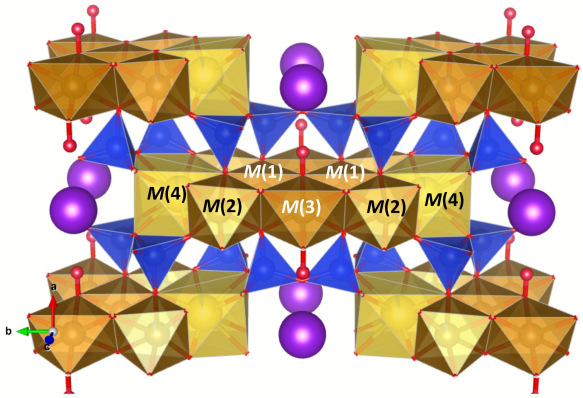

Fig. 1 The crystal structure of potassic-ferro-richterite projected along [001]. Hydrogen atoms are the red spheres, while the tetrahedra occupied by Si are in blue, and the alkali sites in violet. Drawing produced using Vesta.[14]

Density Functional Theory calculations of the richterite band structure were performed using the single-crystal structure collected at RT and at selected high temperatures by Oberti et al.[17]. Technical details can be found in the supplementary materials.

Results

XANES spectra collected during the heating experiments are shown in Figure 2, arranged in order of increasing T from top to bottom. Fe K-edge spectra were obtained after subtracting a linear background before the edge and normalising the absorption coefficient to one for the atomic absorption on the average value in the spectral region above 7,150 eV. The two

magnified insets show changes in the fine structure in the critical spectral regions.

Table 1 Refined site populations at the *M*(1,3) octahedra for the investigated crystal sample at RT and at HT.[17]

	Fe^{2+}(RT)	Fe^{3+}(RT)	Ratio Fe^{3+}/Fe_{tot}	Fe^{2+}(HT)	Fe^{3+}(HT)	Ratio $Fe^{3+}/_{tot}$
M(1)	1.81	0.19	0.10	0.25	1.75	0.88
M(2)	1.53	0.47	0.24	1.42	0.58	0.29
M(3)	0.87	0.13	0.13	0.95	0.05	0.05
Total	4.21	0.79	0.16	2.62	2.38	0.48
Total XAS			0.36 ± 0.03			0.52 ± 0.01

It is well known that the energy of the absorption edge of transition elements shifts to higher values when the oxidation state increases. Inspection of Figure 2 clearly shows a shift of the spectra towards high energy with increasing temperature. This evidence confirms the expected evolution of the Fe^{3+}/Fe_{tot} ratio that, based on the data reported by Oberti et al.[17], changes from ~0.16 to ~0.5 apfu (atoms per formula unit) during heating. Focussing on the local structure, the oxidation of one Fe^{2+} ion to Fe^{3+} corresponds to a contraction of the metal-oxygen distance in the involved octahedron. Oberti et al.[17] showed that the oxidation of iron selectively occurs at the *M*(1) octahedra, so that the associated strain propagates along the strip of octahedra. The site populations in the three independent octahedra calculated before and after annealing[17] are reported in the first four lines of Table 1.

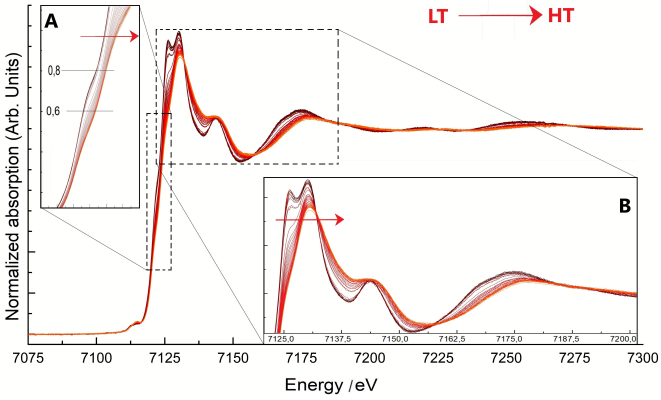

Fig. 2 XANES spectra of synthetic potassic-ferro-richterite collected at the Fe K-edge vs. temperature. Panel (A) shows the zoom on the edge region showing the 0.6 and 0.8 transects used to evaluate the energy shift vs. temperature (see Fig. 4); panel (B) shows a zoom of the MS region. Arrows indicate the increasing temperature from RT to ~ 750° C.

Other significant modifications in the spectral pattern at the Fe K-edge at the white line and in the Multiple Scattering (MS) region above 7140 eV are detectable. As shown in the inset B of Figure 2, the first MS structure above 7140 eV decreases in intensity, broadens and shifts to higher energy because of both the disorder induced by the temperature and the simultaneous contraction of the octahedra where the iron oxidation occurs. Similarly, the shape resonance between 7170 and 7180 eV is smeared and shifted to high energy.

A preliminary quantitative analysis of the Fe^{3+}/Fe_{tot} ratio can be obtained looking at the energy shift of the edge vs. temperature, at the height of 0.8 and 0.6 of the normalized absorption cross section shown in Figure 2.

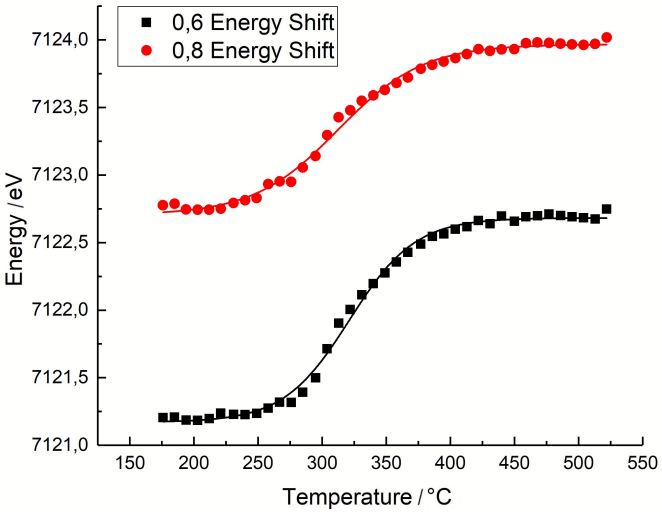

Fig. 3 Fit of the Fe K-edge behaviour vs. temperature of the spectra in Fig. 2 calculated at the absorption value of 0.8 (top) and 0.6 (bottom), after normalization above the edge.

Fitting the two datasets (Figure 3) with a sigmoidal Boltzmann curve we obtain an oxidation temperature for iron of 321° ± 2° C and 312° ± 5° C for the 0.6 dataset and the 0.8 dataset, respectively. However, these estimations can be affected by errors because these experimental spectra result from the overlapping of Fe K-edge spectra relative to three different *M* sites with variable amounts of Fe^{3+} and Fe^{2+} electronic configurations. The same complexity holds true for the analysis of the MS features of the XANES spectra.[32-34]

This structural complexity is typical of amphiboles and many other silicates, notable micas.[35] To overcome this issue, we tried to evaluate the amount of Fe^{2+} and Fe^{3+} from the changes in the pre-edge features in the temperature range from RT up to 750° C. The analysis of the valence and the relative amounts of the different iron configurations from the analysis of the weak pre-edge structure is an old method pioneered by Bajt et al.,[36] and later used by many other authors such as Wilke et al.,[37] Petit et al.[38] and Berry et al.[39] and recently reconsidered using univariate and multivariate approaches in amphiboles by Dyar et al.[8]

Figure 4 shows the evolution of the pre-edge features vs. temperature from 90° C up to 750° C. For each XANES spectrum we extracted a baseline, which simulates the trend of the increase in the cross section before the white line, using an arctangent function (all details of the procedure of extraction and normalization of the pre-edge spectra are provided in the supplementary materials). The pre-edge spectrum contains the contributions from iron ions with different valences and coordination states due to quadrupolar transitions in a distorted centro-symmetric coordination. Crystal-field theory states that the electronic excitation processes in ions with octahedral coordination are

characterized by two possible transitions, leading from the core 1s to the t_{2g} and e_g states.

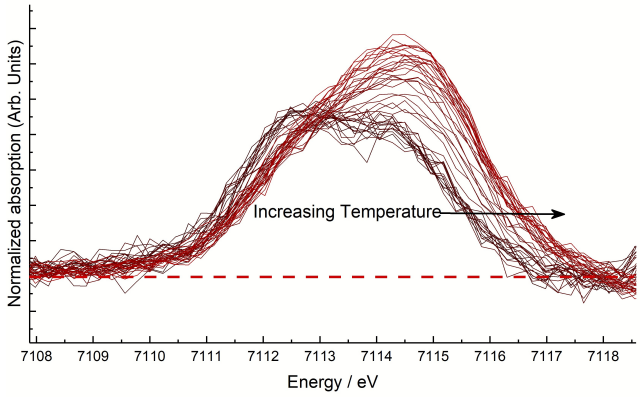

Fig. 4 Zoom of the spectra in Fig. 2 in the pre-edge energy range (7105 eV to 7119 eV) after the subtraction of an arctangent function (see the supplementary materials). The behaviour vs. T is outlined in colour going from left (dark brown = RT) to right (red = HT).

Since our system is a complex mixture with different iron sites we considered two contributions for both the Fe^{2+} and Fe^{3+} ions: 1s $\rightarrow$ t_{2g} and 1s $\rightarrow$ e_g. The pre-edge features showed in Fig. 4 were thus fitted using four Gaussian contributions, corresponding to the above transitions. The ratio of the areas corresponding to these four components should describe the evolution vs. temperature of the relative percentages of the Fe^{3+} and Fe^{2+} configurations during the oxidation induced by thermal annealing. Concerning this issue, we note that according to the structural work of Oberti et al.[17] the involved *M*(1,2,3) octahedra are relatively regular at RT (see Table S1). When increasing T, they modify their geometry first due to the thermal expansion and then to Fe oxidation that, however, occurs almost exclusively at *M*(1). All bond-lengths changes, for increasing T, are ≤ 5% except *M*(1)-O(3) whose change is however ~8%. Changes in polyhedral geometry due to Fe oxidation are more significant especially when involving the O(1) and O(3) oxygens, and may even reach 8.4% in the case of the *M*(1)-O(3) distance (see Table S1). As a consequence, the energy splitting among iron energy states of all M sites can be considered almost overlapping. In addition, according to the work of Oberti et al.[20] and the Mössbauer data of Redhammer and Roth[29], no contributions from the *M*(4) site is expected in the pre-edge spectra, due to the negligible amount of Fe present at this site (< 1% over total Fe). The fitting model based on four contributions is then suitable for treating our data and in good agreement with DFT calculations based on the structural data of Oberti et al.[17]. Indeed the projected d density of states of octahedral coordinated Fe^{2+} and Fe^{3+} are well separated (energy difference $\Delta_{eg\text{-}t2g}$ ~ 1.7 eV at RT) and remains separated at HT.
Figure 6 shows the evolution with T of the Fe^{3+}/Fe_{tot} ratio, obtained integrating the fitted peak areas. If the area of each Gaussian component is expressed as A_1, A_2, A_3 and A_4, where A_3 and A_4 refer to contributions of Fe^{3+}, we may obtain the Fe^{3+}/Fe_{tot} ratio (R) as:

$$R=(A_3+A_4)/(A_1+A_2+A_3+A_4) \quad (2)$$

Figure 5 shows that Fe oxidation starts around 300° C and is completed within a temperature range of ~100° C, in good agreement with previous XRD experiments[17] done on a single crystal, although on a much longer time scale (~2 days). The calculated onset temperature of Fe oxidation is 310 °C ± 4 °C. Understanding the mismatch between the total increase of the Fe^{3+}/Fe_{tot} ratio before and after the heating experiment, as provided by XAS and XRD (~0.15 vs. ~0.32, respectively), and the substantial difference among the values of this ratio: 0.16 vs. 0.41 and 0.48 vs. 0.56 (Table 1) is a crucial issue. Indeed the possibility of quantifying the Fe^{3+}/Fe_{tot} ratio in minerals is one of the goals of the present work, and would represent an important advancement for crystal-chemical studies.

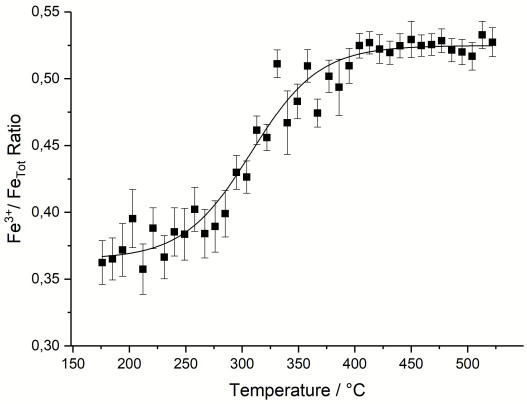

Fig. 5 – Evolution of the Fe^{3+}/Fe_{tot} ratio from our analysis of the pre-edge spectra at the Fe K-edge.

At present, the reason for this discrepancy remains unclear. In principle, it might be related to a significant inhomogeneity of the samples studied by us and by previous authors. According to the original description of Redhammer and Roth[29], their experiments gave run products with different Fe^{3+}/Fe^{2+} compositions, a feature that is common in Fe-bearing systems, due to the difficulty in properly buffering the redox conditions during synthesis[40]. Previous work (see for example Ref.s 40 and 41) shows that, when synthesizing amphiboles, the resulting compositions may depart significantly from the expected ones, and the run products may be strongly inhomogeneous. This work was done on powders obtained by grinding a large number of crystallites, and thus the Fe^{3+}/Fe_{tot} of our sample can be different from that measured by Oberti et al.[17]. We can anticipate that a similar analysis of the Fe^{3+}/Fe_{tot} done on the same riebeckite sample studied by Oberti et al.[20] and Della Ventura et al.[21] provided a Fe^{3+}/Fe_{tot} ratio in excellent agreement with that obtained in the previous works. In this case, however, fragments of a highly homogeneous large crystal could be used for all experiments, and this may guarantee a proper cross-calibration for all used techniques.
As emphasized in the introduction, the amphibole supergroup includes a great number of species with very different compositions, the HT behaviour of which has not yet been completely clarified but surely varies significantly[16-22]. In general, amphiboles respond to the increase in temperature in three distinct ways which can now be easily detected and

interpreted by XRD: (1) thermal expansion; (2) cation disorder and (3) deprotonation, which in turn implies oxidation of Fe^{2+} to Fe^{3+} mostly at the *M*(1) and partly at the *M*(3) site.

In order to get further insight into these processes, XAS data were compared to the XRD data obtained on the same sample during the same experiment. These latter data were also compared to those obtained by single-crystal XRD analysis.[17] Although the diffraction data collected with our setup do not have the same quality as those of Oberti et al.[17], yet they allow monitoring the variation of the unit cell parameters as a function of temperature. As expected, and in agreement with Ref. 17, the volume of the unit cell first increases because of thermal expansion and an abrupt transition is observed around 300° C due to the onset of oxidation/deprotonation. Actually, all the unit-cell edges (*a*, *b*, *c*), and the monoclinic angle β were irreversibly modified during the heating process. In particular, *a*, *b*, and *c* increase while, as a response to the thermal expansion, β decreases in the initial stage of the thermal treatment. Interestingly, as already observed using single-crystal XRD[17], around 300° C we observe an anomalous increase in the β angle. This observation points out a structural adjustment, consisting of a chain sliding, needed to compensate the local strains induced by the contraction of the *M*(1) octahedra caused by Fe^{2+} oxidation.

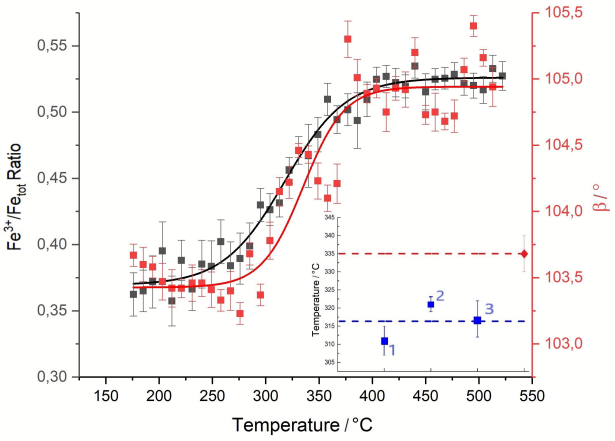

Fig. 6 – Comparison of the evolution of the Fe^{3+}/Fe_{tot} ratio (black) and the β angle (red) vs. temperature. The inset shows the different transition temperatures obtained by XAS (blue) and XRD (red) measurements. The blue line is the average among the different evaluation procedures done on XAS spectra. The red diamond corresponds to the value obtained by the variation of the β angle[17].

Figure 6 compares the results from the two simultaneous XAS and XRD experiments; although the relatively large error associated with the data points, the variation of β (from XRD patterns) and of the Fe^{3+}/Fe_{tot} ratio (evaluated from the pre-edge analysis of the XAS spectra) clearly follow the same trend. However, the transformation temperature calculated from XRD is 335 ± 5 °C, i.e. ~20 °C higher than that obtained by the analysis of the pre-edge of the XAS spectra. Because the two experiments were done simultaneously, this finding points out clearly, and for the first time, that iron oxidation starts ~20° C before the structural adjustment occurring at the long-range scale. In other words, it suggests that the electronic transitions proceeds and trigger the structural changes. The inset in Figure 6 shows in blue the temperatures of the transitions evaluated by the different methods used to model the XAS spectra, i.e., the energy shift at 0.6 and 0.8 % of the edge (method 1 and 2, respectively), and the fit of the pre-edge region (method 3). It is noteworthy that all the three methods, within the experimental error, provide close transition temperatures (optimized by the blue line). Therefore, the temperature of the iron oxidation for this Fe-amphibole is slightly higher than 315 °C, well below the temperature of ~335 °C obtained by XRD (red line) which however refers to the long-range structural adjustments consequent to massive Fe oxidation.

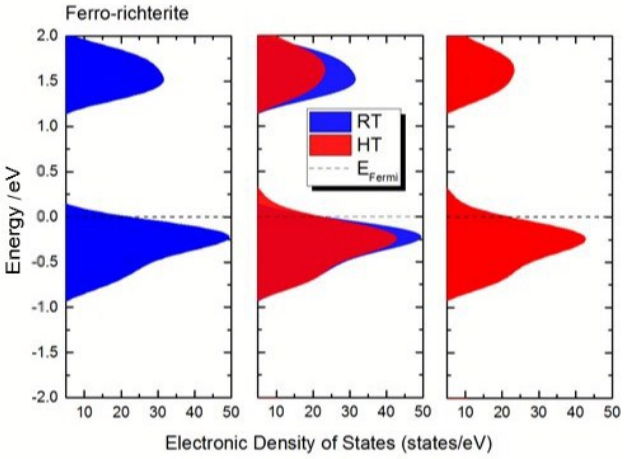

Fig. 7 - Comparison of the density of states (DOS) in the vicinity of the Fermi energy for potassic-ferro-richterite computed at RT and at HT from the XRD structural data of Oberti et al.[17].

The effect of iron oxidation on the calculated density of states of potassic-ferro-richterite is given in Figure 7. Following the loss of hydrogen in the high-temperature phase, there is a metal to insulator transition as shown by the extra DOS above the Fermi energy. Analysis of the band structure shows that an indirect band gap of 1.3 eV characterizes the RT phase while the HT phase is metallic (see also Figure S6 in supplementary materials). The conduction band above the Fermi energy is occupied by electrons made available by the iron oxidation process. Summarizing, all experimental data are in agreement with a multi-step process, where the response to increasing T involves different parts of the amphibole structure: the shrinking of the *M*(1) octahedra formerly occupied by Fe^{2+}, the loss of hydrogen at the anionic O(3) site and the migration or diffusion of hydrogen or hydrogen/oxygen species with the consequent formation of water molecules at the sample surface. The same conclusion was reached recently on the Fe-rich amphibole riebeckite by combining XRD, Mössbauer and vibrational (FTIR, Raman) spectroscopy data.[21] In particular, detailed analysis of the temperature dependence of the wavenumber and FWHM of selected phonon modes involving both M-O and Si-O vibrations clearly showed that, at a local

scale, delocalization of e^- and H^+, consequent to the Fe^{2+} oxidation, precedes and possibly trigger the structural adjustments in the silicate chains. The approach followed in this work is straightforward and more reliable because all measurements were simultaneously done on the same sample and in the same experimental conditions.

Conclusions

This work is a further step towards the complete understanding of the complex dynamics of Fe oxidation in hydroxyl silicates. From a methodological point of view, it shows that modelling of the process is significantly improved by the simultaneous collection of short-range and long-range scale information. Also, a careful analysis of both the pre-edge and edge features does allow characterizing all local electronic and structural changes associated to the variation of the Fe^{3+}/Fe_{tot} ratio in these complex minerals. In this case the results of the method point out a mismatch between the value of the Fe^{3+}/Fe_{tot} provided by XAS and XRD that needs to be clarified. Indeed the calibration of this original approach based on the analysis of the pre-edge of the XAS spectra at the Fe K-edge may become a powerful tool for the investigation of many crystal-chemical processes. Additional investigations in other iron-based silicates are in progress to measure and calibrate the method.

Finally, the results of this work clearly support models of conductivity of amphibole-bearing rocks, which do not require conductive fluids.[15] In fact, they show that conductivity may increase simply due to the oxidation of iron. In-situ experiments should be planned to probe and measure the enhancement of the conductivity during heating. The data presented here and the recent work from Della Ventura et al.[21] shows that the loss of hydrogen after HT annealing does follow the oxidation of iron. Therefore, when the amphibole is completely oxidized (in the present case, beyond 800° C) its conductivity disappear. This feature could affect existing models on the role of Fe-bearing, hydrous minerals, on the electrical conductivity at lower-crust/mantle conditions. A better comprehension of these phenomena, and the connection between crystal-chemistry and physical-chemistry is therefore mandatory for an improved geophysical modelling of the Earth.

The approach presented here is based on the simultaneous use of two independent techniques, a procedure that has been rarely applied in this context, where HT processes of multiple-valence elements are involved. We point out that only using simultaneous XRD and XANES techniques we can try discriminating the mechanism behind the HT oxidation processes of iron in silicates, identify the driving force for this irreversible transformation and determine the temperature range where this process can be eventually reversible. This work does no add just another piece of information in the characterization of the sample, but attempts to reconstruct for the first time the dynamics behind this quite unique oxidation process.

Conflicts of interest

There are no conflicts to declare.

Acknowledgements

We thank Diamond Light Source for access to beamline B18 (proposal number NT12031). W.X. is financially supported by the National Science Foundation of China (Grants no. U1532128). W.X. acknowledges the financial support and the hospitality of LNF under the framework of IHEP&INFN collaboration agreement in 2015-2017. W.X. acknowledges Wencai Yi for his tool qvasp. Part of the DOS calculations here presented have been obtained on the "Era" petascale supercomputer of the Computer Network Information Center of the Chinese Academy of Sciences.

Notes and references

1 C. Bonadiman, S. Nazzareni, M. Coltorti, P. Comodi, G. Giuli B. Faccini, Crystal chemistry of amphiboles: implications for oxygen fugacity and water activity in lithospheric mantle beneath Victoria Land Antarctica, *Contributions to Mineralogy and Petrology*, 2014, **167-3**, 1-17.

2 F.C. Hawthorne, Mössbauer Spectroscopy, *Rev. Mineral*., 1983, **18**, 255-340.

3 G. Della Ventura, G. Iezzi, G.J. Redhammer, F.C. Hawthorne, B. Scaillet, D. Novembre, Synthesis and crystal-chemistry of alkali amphiboles in the system Na_2O-MgO-FeO-Fe_2O_3-SiO_2-H_2O as a function of fO_2, *Amer. Mineral.*, 2005, **90**, 1375–1383.

4 G. Della Ventura, G.J. Redhammer, G. Iezzi, F.C. Hawthorne, A. Papin, J.L. Robert, A Mössbauer and FTIR study of synthetic amphiboles along the magnesioriebeckite – ferri-clinoholmquistite join, *Phys. Chem. Miner.*, 2005, **32**, 103–113.

5 C.A. McCammon, A Mossbauer milliprobe: practical considerations, *Hyperfine Int*., 1994, **92**, 1235-1239.

6 W.M. Lamb, R. Guillemette, R.K. Popp, S.J. Fritz, G.J. Chmiel, Determination of the Fe3+/Fe using the electron microprobe: A calibration for amphiboles, *Am. Mineral*., 2012, **97**, 951-961.

7 C. Wagner, E. Deloule, M. Fialin, P.L. King, Dehydrogenation of kaersutitic amphibole under electron beam excitatio recorded by changes in $Fe^{3+}/\sum Fe$: An EMP and SIMS study, 2008, *Am. Mineral*., **93**, 1273–1281

8 M. Darby Dyar, E.A. Breves, M.E. Gunter, A. Lanzirotti, J.M. Tucker, C.J. Carey, S.E. Pee, E.B. Brown, R. Oberti, M. Lerotic, and J.S. Delaney, Use of multivariate analysis for synchrotron micro-XANES analysis of iron valence state in amphiboles, *Am. Mineral*., 2016, **101**, 1171–1189

9 G. Giuli, E. Paris, G. Pratesi, C. Koeberl, C. Cipriani, Iron oxidation state in the Fe-rich layer and silica matrix of Libyan Desert Glass: A high-resolution XANES study, Meteoritics and Planetary Science, 2003, **38**, 1181-1186.

10 C.C. Addison, W.E. Addison, G.H. Neal, J.H. Sharp, Amphiboles. Part I. The oxidation of crocidolite, *J. Chem. Soc.*, 1962, 1468-1471.

11 W.E. Addison, G.H. Neal, and J.H. Sharp, Amphiboles. Part II. The kinetics of oxidation of crocidolite, *J. Chem. Soc.*, 1962, 1472-1475.

12 W.E. Addison, and J.H. Sharp, Amphiboles. Part III. The reduction of crocidolite. *J. Chem. Soc.*, 1962, 3693-3698.

13 W.G. Ernst, and M. Wai, Mössbauer, infrared, X-ray and optical study of cation ordering and dehydrogenation in natural and heat-treated sodic amphiboles. *Am. Mineral*, 1970, **55**, 1226-1258.

14 K. Momma, and F. Izumi, Vesta 3 for three-dimensional visualization of crystal, volumetric and morphology data. *J. App. Cryst*., 2011, **44**, 1272-1276.

15 D. Wang, Y. Guo, Y. Yu, and S. Karato Electrical conductivity of amphibole-bearing rocks: influence of dehydration. *Contrib. Mineral. Petrol*., 2012, **164**, 17-25.

16 M.D. Welch, F. Cámara, G. Della Ventura, G. Iezzi, Non-ambient in situ studies of amphiboles. *Reviews in Mineralogy and Geochemistry*, 2007, **67**, 223-260.

17 R. Oberti, M. Boiocchi, M. Zema, G. Della Ventura, Synthetic potassic-ferro-richterite: 1. Composition, crystal-structure and HT behaviour by in operando single-crystal X-ray diffraction. *Can. Mineral*., 2016, **54**, 353-369.

18 M.D. Welch, F. Cámara, and R. Oberti, R., Thermoelasticity and high-T behaviour of anthophyllite. *Phys. Chem. Miner*, 2011, **38**, 321-334.

19 M. Zema, M.D. Welch, and R. Oberti, R., High-T behaviour of gedrite: thermoelasticity and dehydrogenation, *Contrib. Mineral. Petrol.*, 2012, **163**, 923-937.

20 R. Oberti, M. Boiocchi, M. Zema, F.C. Hawthorne, G.J. Redhammer, U. Susta, G. Della Ventura G., Understanding the peculiar HT behavior of riebeckite: espansivity, deprotonation, Fe-oxidation and a novel cation disorder scheme, *Eur. J. Mineral.,* 2018, DOI: 10.1127/ejm/2018/0030-2712.

21 G. Della Ventura, B. Milahova, U. Susta, M. Cestelli Guidi, A. Marcelli, J. Schlüter, R. Oberti, The dynamics of Fe oxydation in riebeckite: a model for amphiboles, *Am. Mineral.,* 2018*, **103,** in press*.

22 G. Della Ventura, U, Susta, F. Bellatreccia, A. Marcelli, G.J. Redhammer, R. Oberti, R. Deprotonation of Fe-dominant amphiboles: Single-crystal HT-FTIR spectroscopic studies of synthetic potassic-ferro-richterite. *Am. Mineral.,* 2017, **102**, 117-125. DOI: 10.2138/am-2017-5859

23 E. Schmidbauer, Th. Kunzmann, Th. Fehr, R. Hochleitner, Electrical resistivity and 57Fe Mossbauer spectra of Fe-bearing calcic amphiboles. Phys. Chem. Miner., 2000, **27**, 347-356.

24 P. Innocenzi, T. Kidchob, J. Mio Bertolo, M. Piccinini, M. Cestelli Guidi and A. Marcell, Time-Resolved Infrared Spectroscopy as an In Situ Tool To Study the Kinetics During Self-Assembly of Mesostructured Films, *J. Phys. Chem. B*, 2006, **110**, 10837-10841.

25 P. Innocenzi, L. Malfatti, T. Kidchob, S. Costacurta, P. Falcaro, M. Piccinini, A. Marcelli, P. Morini, D. Sali and H. Amenitsch, Time-Resolved Simultaneous Detection of Structural and Chemical Changes during Self-Assembly of Mesostructured Films, *J. Phys. Chem. C*, 2007, **111**, 5345

26 A. Marcelli, D. Hampai, Wei Xu, L. Malfatti and P. Innocenzi, Time resolved IR and X-ray simultaneous spectroscopy: new opportunities for the analysis of fast chemical-physical phenomena in materials science, *Acta Phys. Pol. A*, 2009, **115**, 489-500.

27 Wei Xu, A. Marcelli, D. Hampai, L. Malfatti, P. Innocenzi, U. Schade and Ziyu Wu, New opportunity to investigate physico-chemical phenomena: time resolved X-ray and IR concurrent analysis, *Ren. Accad. Lincei*, 2011, **22**, S59-S79.

28 A. Marcelli, P. Innocenzi, L. Malfatti, M.A. Newton, J.V. Rau, E. Ritter, U. Schade, Wei Xu, IR and X-ray time resolved simultaneous experiments: an opportunity to investigate the dynamics of complex systems and non-equilibrium phenomena using 3rd generation synchrotron radiation sources, *J. Synchrotron Rad*., 2012, **19**, 892-904.

29 G.J. Redhammer, and G. Roth, Crystal structure and Mössbauer spectroscopy of the synthetic amphibole potassic-ferri-ferrorichterite at 298 K and low temperatures (80–110 K). *Eur. J. Mineral*., 2002, **14**, 105-114.

30 F.C. Hawthorne, R. Oberti, G.E. Harlow, W.V. Maresch, R.F. Martin, J.C. Schumacher, M.D. Welch, Nomenclature of the amphibole supergroup. *Am. Mineral*., 2012, **97**, 2031-2048.

31 B. Schmitt, Ch. Bronnimann, E.F. Eikenberry, F. Gozzo, C. Hormann, R.Horisberger, B. Patterson, Mythen detector system, *Nucl. Instr. Meth. Phys. Res. A*, 2003, 267–272.

32 F. Galdenzi, Master thesis, University "Tor Vergata" (Rome, July 2017) unpublished.

33 C. Piquer, M.A. Laguna-Marco, A.G. Roca, R. Boada, C. Guglieri and J. Chaboy, Fe K-Edge X-ray Absorption Spectroscopy Study of Nanosized Nominal Magnetite, J. Phys. Chem. C, 2014, **118**, 1332-1346

34 M.A. Soldatov, J. Göttlicher, S.P. Kubrin, A.A. Guda, T.A. Lastovina, A.L. Bugaev, Yu.V. Rusalev, A.V. Soldatov and C. Lamberti, Insight from X-ray Absorption Spectroscopy to Octahedral/Tetrahedral Site Distribution in Sm-Doped Iron Oxide Magnetic Nanoparticles, J. Phys. Chem. C, 2018, **122**, 8543-8552.

35 F. Tombolini, M.F. Brigatti, A. Marcelli, G. Cibin, A. Mottana and G. Giuli, Local and average Fe distribution in trioctahedral micas: Analysis of Fe K-edge XANES spectra ion the phlogopite-annite and phlogopite-tetra-ferriphlogopite joins on the basis of single-crystal XRD refinements, *Eur. J. Mineral*., 2002, **14**, 1075-1085.

36 S. Bajt, S.R. Sutton, J.S. Delany, X-ray microprobe analysis of iron oxidation states in silicates and oxides using X-ray absorption near edge structure (XANES). *Geochim. Cosmochim. Acta*, 1994, **58**, 5209-5214.

37 M. Wilke, F. Farges, P.E. Petit, G.E. Brown Jr., F. Martin, Oxidation state and coordination of Fe in minerals: an Fe K XANES spectroscopic study. *Am. Mineral*., 2001, **86**, 714-730.

38 P.E. Petit, F. Farges, M. Wilke, M., V.A. Solé, Determination of the iron oxidation state in Earth materials using XANES pre-edge information. *J. Synchrotron Rad*., 2001, **8**, 952-954.

39 A.J. Berry, H.St.C. O'Neill, K.D. Jayasuriya, S.J. Campbell, G.J. Foran, XANES calibration for the oxidation state of iron in a silicate glass. *Am. Mineral.*, 2003, **88**, 967-977.

40 G. Iezzi, F. Cámara, G. Della Ventura, R. Oberti, G. Pedrazzi, J.L. Robert, Synthesis, crystal structure and crystal-chemistry of ferri-clinoholmquistite, $Li_2Mg_3Fe^{3+}{}_2Si_8O_{22}(OH)_2$. *Phys. Chem. Miner*., 2003, **31**, 375-385.

41 G. Della Ventura, G. Redhammer, J.L. Robert, J. Sergent, G. Iezzi, A. Cavallo, Crystal-chemistry of synthetic amphiboles along the join richterite - ferro-richterite: a combined spectroscopic (FTIR, Mössbauer), XRPD and microchemical study. Canadian Mineralogist, 2016, **54**, 97-114.